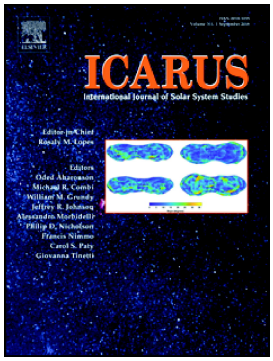

Cryovolcanic flooding in Viking Terra on Pluto

Dale P. Cruikshank, Cristina M. Dalle Ore, Francesca Scipioni, Ross A. Beyer, Oliver L. White, Jeffrey M. Moore, William M. Grundy, Bernard Schmitt, Kirby D. Runyon, James T. Keane, Stuart J. Robbins, S. Alan Stern, Tanguy Bertrand, Chloe B. Beddingfield, Catherine B. Olkin, Leslie A. Young, Harold A. Weaver, Kimberly Ennico

PII: S0019-1035(20)30172-X

DOI: https://doi.org/10.1016/j.icarus.2020.113786

Reference: YICAR 113786

To appear in: *Icarus*

Received date: 15 November 2019

Revised date: 15 March 2020

Accepted date: 30 March 2020

Please cite this article as: D.P. Cruikshank, C.M. Dalle Ore, F. Scipioni, et al., Cryovolcanic flooding in Viking Terra on Pluto, *Icarus* (2020), https://doi.org/10.1016/j.icarus.2020.113786

Revised March 15, 2020

Cryovolcanic Flooding in Viking Terra on Pluto

Dale P. Cruikshank[a*], Cristina M. Dalle Ore[a,b], Francesca Scipioni[a,b], Ross A. Beyer[a,b], Oliver L. White[a,b], Jeffrey M. Moore[a], William M. Grundy[c], Bernard Schmitt[d], Kirby D. Runyon[e], James T. Keane[f], Stuart J. Robbins[g], S. Alan Stern[g], Tanguy Bertrand[a], Chloe B. Beddingfield[a,b], Catherine B. Olkin[g], Leslie A. Young[g], Harold A. Weaver[e], Kimberly Ennico[a]

[a]NASA Ames Research Center. Moffett Field, CA, United States
[b]SETI Institute, Mountain View, CA, United States
[c]Lowell Observatory, Flagstaff, AZ, United States
[d]Université Grenoble Alpes, CNRS, IPAG, Grenoble, France
[e]Applied Physics Laboratory, Johns Hopkins University, Laurel, MD, United States
[f]California Institute of Technology, Pasadena, CA, United States
[g]Southwest Research Institute, Boulder, CO, United States

*Corresponding author:
Dale P. Cruikshank, Dale.P.Cruikshank@nasa.gov

Key Words:
Pluto, Volcanism, IR spectroscopy, Surface, Ices

ABSTRACT

A prominent fossa trough (Uncama Fossa) and adjacent 28-km diameter impact crater (Hardie) in Pluto's Viking Terra, as seen in the high-resolution images from the New Horizons spacecraft, show morphological evidence of in-filling with a material of uniform texture and red-brown color. A linear fissure parallel to the trough may be the source of a fountaining event yielding a cryoclastic deposit having the same composition and color properties as is found in the trough and crater. Spectral maps of this region with the New Horizons LEISA instrument reveal the spectral signature of H_2O ice in these structures and in distributed patches in the adjacent terrain in Viking Terra. A detailed statistical analysis of the spectral maps shows that the colored H_2O ice filling material also carries the 2.2-μm signature of an ammoniated component that may be an ammonia hydrate ($NH_3 \bullet nH_2O$) or an ammoniated salt. This paper advances the view that the crater and fossa trough have been flooded by a cryolava debouched from Pluto's interior along fault lines in the trough and in the floor of the impact crater. The now frozen cryolava consisted of liquid H_2O infused with the red-brown pigment presumed to be a tholin, and one or more ammoniated compounds. Although the abundances of the pigment and ammoniated compounds entrained in, or possibly covering, the H_2O ice are unknown, the strong spectral bands of the H_2O ice are clearly visible. In consideration of the factors in Pluto's space environment that are known to destroy ammonia and

ammonia-water mixtures, the age of the exposure is of order $\leq 10^9$ y. Ammoniated salts may be more robust, and laboratory investigations of these compounds are needed.

1. Introduction and background

Several structures on Pluto's surface seen in the images and supported by spectroscopic data from the New Horizons spacecraft appear to have originated by cryovolcanic processes. The pronounced constructional edifices known as Piccard Mons (33.2º S, 174º E) and Wright Mons (22.6º S, 171.9º E) south of Sputnik Planitia exhibit high relief and deep central pits, and may be cryovolcanic in origin (Singer et al. 2016, 2018; Schenk et al. 2018). In the broad arc west of Sputnik Planitia called Viking Terra, some tectonic fractures and graben structures appear to be conduits through which cryolavas have emerged onto the surface from one or more subsurface reservoirs. This region falls within a zone of large-scale crustal fracturing that has occurred from a concentration of stress by factors in the planet's history including true polar wandering, freezing of a global subsurface ocean, and crustal loading by the nitrogen glacier in Sputnik Planitia (Keane et al. 2016). The magnitude of the stress, calculated by Keane and colleagues, is shown in the global map of Pluto in Fig. 9 of Cruikshank et al. (2019), and is maximum in an arc that includes the main parts of the planet covered by H_2O ice in maps by Schmitt et al. (2017) and Cook et al. (2019).

For a site of cryovolcanism in Pluto's Virgil Fossae, Cruikshank et al. (2019) drew the connection between the surface exposure of H_2O ice that carries the spectral signature of ammonia in some form, and the effect of ammonia in a subsurface fluid reservoir on the long-term retention of liquid in the interior of the planet. They further noted that ammonia-induced pressurization of the fluid reservoir is likely to have opened conduits to the surface. New calculations by Martin and Binzel (2020) demonstrate that this is a viable mechanism. Below, in the present paper we show that the site in Viking Terra described here also shows spectroscopic evidence of ammoniated H_2O, and appears to represent a location where fluid has emerged onto the surface and filled a crater and fossa trough.

2. Viking Terra site

Figures 1 and 2 show a large section of Viking Terra, with the Al Idrisi mountains to the east (right side of images). In addition to the large number of craters, this region is incised by several fossae; the northern-most is Inanna Fossa, and the southern structure running nearly parallel to Inanna is Dumuzi Fossa, while the arc-shaped fossa complex to the south is named Uncama Fossa and is the subject of this paper. Here we explore a site of possible cryovolcanic activity north of Virgil Fossae (VF)and its immediate surroundings in Viking Terra, and especially in this fossa complex.

FIGURE 1 HERE

Fig. 1. A region in Viking Terra imaged with the New Horizons Multispectral Visible Imaging Camera (MVIC), with the color (shown in brown) artificially enhanced to show

contrasts in the albedo and color differences in the geological and geographical structures. The principal geological features discussed in this paper are (a) the flooded crater Hardie, (b) the filled fossa trough (Uncama Fossa), and (c) the fissure and associated cryoclastic deposit. (For interpretation of the references to color in this figure, the reader is referred to the web version of this article.)

FIGURE 2 HERE

Fig. 2. The distribution of H_2O ice (blue) in this section of Viking Terra is shown by the superposition of the map of H_2O ice from Schmitt et al. (2017) on the base map (black and white monochrome). The H_2O spectral index is the depth of the 2.08-μm H_2O band relative to the continuum around 1.39 μm, as defined in Schmitt et al. (2017); higher values (darker blue color) indicate stronger absorption in the major H_2O spectral bands measured in data taken with the LEISA (Linear Etalon Infrared Spectral Array) instrument. (For interpretation of the references to color in this figure, the reader is referred to the web version of this article.)

The spectral images from New Horizons analyzed by Protopapa et al. (2017), Schmitt et al. (2017), and Cook et al. (2019) all show exposures of H_2O ice and the coloration that it carries in many places in the section of Viking Terra illustrated in Figures 1 and 2. Some of these are in the interiors of craters whose rims appear to be dusted with a high-albedo frost of CH_4, apparently deposited by the atmosphere in annual and longer cycles of condensation and sublimation (Bertrand et al. 2019). Additional exposures of the colored H_2O are seen in craters and fossae, while still other exposures are found where there is little distinguishing topography that would serve as clues to the origin or emplacement of the H_2O ice. We have focused the present investigation on a limited area where two distinct topographic structures, a crater (Hardie) and a fossa trough (Uncama Fossa), appear to present a clear and unambiguous picture of one or more events pointing to a plausible event of filling from a subsurface source of fluid. A third nearby feature is a fissure ~80 km long (Figure 4), running nearly parallel to the fossa, and appearing as a possible source of a cryoclastic deposit on the surrounding terrain. In Figure 3 these features are denoted "a", "b", and "d", respectively

FIGURE 3 HERE

Figure 3. The embayed or flooded crater (a) named Hardie, the adjacent main trough of Uncama Fossa (b), and the 80-km fissure (d) in Viking Terra. (c) is the double crater referenced later in this paper. Three arrows at the distal end of small troughs mark sites of apparent ponding of the same material filling the trough and crater. (For interpretation of the references to color in this figure, the reader is referred to the web version of this article.)

FIGURE 4 HERE

Figure 4. Fissure with surrounding apron of ammoniated, colored H_2O ice, labeled "d" in Figure 3. Contrast enhanced image with the Long Range Reconnaissance Imager

(LORRI) in a pass over a central region of Pluto and optimized for LEISA spectral images at high spatial resolution (LORRI_P_LEISA_HIRES).

In the section of the main trough of Uncama Fossa running from northwest to southeast there is a ~100-km reach that is mostly filled with colored material. An adjacent 28-km Hardie crater has been filled or embayed with the same material. At the southeast extremity, there are three, possibly four, narrow troughs about 40-50 km long, and the same colored material seems to have ponded at the eastern (distal) ends of at least two of them. The digital elevation model (Schenk et al. 2018) does not reliably resolve irregularities in the surface textures of the crater and the filled trough, but in the best images (designated LORRI P_LEISA_HIRES) with resolution 232 m/pixel the surfaces appear uniform. The uniform upper surface of both the crater and the filled fossa suggests that the surface of the infill material lies at the same depth in the trough as it does in the crater, and that the filling material was originally a fluid. In support of this view, elevation transects across the region and the topographic features show that the surface of the fossa filling material and that in the crater lie at the same depth below the local terrain (Fig. 5a).

Adjacent to the fissure (Figs. 3 and 4), some small craters are mantled with the same colored H_2O ice as the fossa and the larger embayed crater. The fissure may be the site of a cryoclastic fountaining event that left a deposit extending ~30 km onto the surrounding terrain. As noted in Cruikshank et al. (2019), simple ballistic trajectories of fountain ejecta on Pluto can travel a few hundred kilometers from the source with reasonable vent velocities substantially lower than the planet's escape velocity. Stereo imagery in this region with New Horizons does not allow a reliable estimate of the thickness of the mantling layer, but the visibility of several affected craters and the profile across the fissure (Figure 5a) suggest that it is probably somewhat less than 100 m.

These structures abut (or are a part of) the north-south ridge-trough system described by Schenk et al. (2018). We further note the detection of the spectral signature of ammonia or ammoniated compounds, as well as a distinctive pigment, in the H_2O ice, supporting the contention that a fluid with these characteristics emerged through lines or zones of structural crustal weakness (see below). This analysis builds on our earlier study of Virgil Fossae (VF), where crustal fractures comprising the fossa complex cut through the north rim of Elliot crater, and are seen in New Horizons data as sources of a cryolava consisting of H_2O containing NH_3 or ammoniated compounds, and that is colored by a distinctive red-orange pigment (Cruikshank et al. 2019a,b).

Four factors draw our attention to this particular site: 1) the morphology of the crater, fossa and adjacent linear fissure, 2) the spectroscopic detection of H_2O ice, 3) the color of the icy deposit, and 4) the spectroscopic detection of NH_3 or ammoniated compounds

contained in the colored ice. The issue of the age of the event(s) causing the deposition of material rests on the detection of water ice carrying the spectral signature of an ammoniated compound. These detections are derived from the spectral images of the same region made with the mapping spectrometer (LEISA) on the New Horizons spacecraft. The ammoniated water problem is parallel to that described for Virgil Fossae (Dalle Ore et al. 2019; Cruikshank et al. 2019a), and subject to similar uncertainties, both in terms of the identification of the ammoniated component and the age of emplacement.

The darker-toned regions in Figs. 1, 2, and 3 represent exposures of H_2O ice; in Figs. 1 and 3 these exposures are seen to be colored with a red-brown pigment, interpreted here and for similar exposures elsewhere as a complex organic molecular mix (tholin) (Grundy et al. 2016) (see below). Lighter toned regions, which occur primarily on crater rims, mountains, and other elevated terrains, are covered with CH_4 ice or frost, as seen in maps of the methane distribution by Protopapa et al. (2017) and Schmitt et al. (2017).

Elevation profiles derived from the Pluto digital elevation map (Schenk et al. 2018) running across the flooded crater, the main fossa trough, and the adjacent double crater are shown in Fig. 5(a), with the traces of the transects shown in Fig. 5(b).

FIGURE 5A HERE

FIGURE 5B HERE

Figure 5a and b. (a) Elevation profiles across the flooded crater, the fossa, and an adjacent double crater. The vertical exaggeration of 10x refers to all three transects. (b, left) Map of the traces shown in (a); (b, right) digital elevation map of this region shaded in color for depth. (For interpretation of the references to color in this figure, the reader is referred to the web version of this article.)

3. Volume of the fossa and crater

The original depth of the principal trough of the in-filled fossa is unknown, but if it is comparable to that of the main trough of Virgil Fossae it is ~2 km below the surrounding terrain (Schenk et al. 2018). To estimate the volume of the infilling material, we take the length of the trough as 100 km, the width (from the elevation profile) as 8 km, and the depth of the surface of the infilling material as 1 km. The volume is then 8×10^2 km^3. A very rough estimate of the volume of the material partially filling the adjacent craters, covering the surrounding terrain, and lying in minor fossa troughs is a few times 10^2 km^3, for a total $>10^3$ km^3.

The original depth of the in-filled crater considered here is unknown, but if it is comparable to that of the twin craters of similar diameter on the opposite side of the trench, its original floor lies ~2 km below the surrounding landscape. This value is consistent with the results of a study of the depth-to-diameter relationship of craters on Pluto and Charon by Robbins et al. (2019, submitted). With an original depth of 2 km

and the present level of the smooth surface deposit below the surroundings (~1 km) the thickness of the filling material is ~1 km. The twin craters themselves may be in-filled by some of the same material, in which case their original depths are greater than -2 km. A rough estimate of the volume of the filling material in the flooded crater is 2 x 10^3 km^3. The total volume of material in this area is then a few times 10^3 km^3.

As points of comparison, historical effusive eruptions on Earth have produced comparable or greater volumes of ash and lavas. For example, the estimated volume of India's Deccan Traps is 9.3 x 10^3 km^3 (Bryan et al. 2010) and numerous individual effusive events in the Columbia River Basalt Group have volumes of ~10^3 km^3 or greater (Martin et al. 2005). The Steens basalt in the Columbia Group has an area of ~5 x 10^4 km^2 and reaches a thickness of ~1 km in places. In the case of the Decan Traps, the post-erosional area of the deposits is ~2 x 10^5 km^2, which, taken together with the estimated volume yields an average thickness of ~46 m. As examples in other kinds of eruptions, the debris avalanche in the 1980 eruption of Mount Saint Helens had an estimated volume of 2.8 km^3 and the volume of the cataclysmic eruption of Mount Mazama ~7700 years ago was ~50 km^3 (https://pubs.usgs.gov/fs/2002/fs092-02/). The estimated total volume of Mauna Loa, the largest terrestrial shield volcano, is 4 x 10^4 km^3 (*volcano.oregonstate.edu/mauna-loa*)

4. The spectral signature of ammoniated material(s)

The distinctive morphology and composition (H_2O and color) of the trench and adjacent crater invite further analysis. Because of the potential importance of NH_3 or ammoniated compounds established in the Virgil Fossae study (Cruikshank et al. 2019), we have applied the same technique that revealed the H_2O and NH_3 in Virgil Fossae and surroundings (Dalle Ore et al. 2019) using New Horizons LEISA spectral images to determine the composition of the colored material in the fossa and crater complex noted above.

The technique rests on isolating the pixels in the spectral image having the least amount of volatile ice contamination (CH_4 in the present case) by multiple, recursive applications of a statistical clustering tool focused on the spectral region between 1.85 and 2.2 μm that is sensitive to the signatures of H_2O vs. CH_4 ice. Analogously to the approach described in Dalle Ore et al (2019), gradients in H_2O and ammoniated materials are analyzed by comparing the spectral signature of neighboring regions identified as volatile-ice-poor.

The Viking Terra region is relatively close to Sputnik Planitia and the north hemisphere of Pluto, rich in volatile ices. The level of contamination from CH_4, N_2, and possibly CO can be substantial. Therefore, the first goal of the analysis was to isolate those pixels with the least amount of volatile ice contamination. To achieve this goal we used an unsupervised k-means classification that applied the Calinski-Harabasz (1974) criterion (C-H). In the multidimensional space where each spectrum is a data point, the C-H criterion identifies the number of classes that allows the tightest clusters with the greatest separation, an ideal condition for well-defined clustering. The classification was tuned to the spectral region 1.85-2.2 μm, which is quite sensitive to the presence of volatile (e.g.,

CH_4) versus H_2O ices, and therefore allows discrimination based on composition. The first result of the clustering is shown in Figure 6, where a map of the resulting classes is overlaid on a base map of the region constructed from the highest-resolution images available (Schenk et al. 2018). Only four classes are found to represent the main spectral variability in the region. On the map in Figure 6 it appears that pixels belonging to Cluster 1 (red) coincide with the material of relatively low albedo that is widespread in this region.

The spectral averages of the four classes are shown in Figure 7. Cluster 1 appears as the one with the strongest H_2O signature as shown by the pronounced dip at 1.5 μm and 2.0 μm. Geographically, it coincides with H_2O-rich regions already reported by Protopapa et al. (2017) and Schmitt et al (2017). Spectroscopically, it is similar to the Virgil Fossae (VF) region spectra. However, upon closer scrutiny, the cluster average for class 1 also shows a clear contamination from CH_4 revealed by the weak bands at ~1.35 -~1.42 μm and at ~1.63 -1.83 μm, and the deep, broad absorption at ~2.23 μm.

FIGURE 6 HERE

Figure 6: Map of initial clustering of the region of interest (left), with the key image (right). The three colors in the rectangles at the top correspond to the colored spectral traces in Figure 6. The arrow points to the 28-km crater (Hardie) considered here. The dark diagonal line (lower left) is an artifact, and although it is nearly coincident with the linear fissure discussed in the text, it does not affect the distribution pattern of the spectral clusters. (For interpretation of the references to color in this figure, the reader is referred to the web version of this article.)

FIGURE 7 HERE

Figure 7. Spectra of the cluster averages corresponding to the initial clustering of the region of interest. The map in Figure 6 shows the distribution of the three different clusters. (For interpretation of the references to color in this figure, the reader is referred to the web version of this article.)

In order to remove the CH_4 contamination effectively we isolated those pixels belonging to Cluster 1 from the others and then re-clustered the subset. For the new clustering we adopted the same spectral region as in the first one (1.85 - 2.2 μm) and again applied the CH criterion to determine the best number of classes into which the sample should be subdivided. This time the CH criterion did not yield a clear maximum, which would be the marker of a well-identified number of classes. This is due to the fact that in this region the different classes are very similar in spectral shape and their main distinction is the depth of the features, which progress in a gradual way from one region to the next. Therefore, while there is no ideal number of clusters, we chose six as a number that highlights with sufficient detail the variations from one class to the other and maps the gradient in a clear way. Of the six classes obtained from the classification only two cluster averages, corresponding to clusters 3 and 6, still showed evidence of the CH_4 contamination signature (Figure 8).

FIGURE 8 HERE

Figure 8. Cluster averages corresponding to the re-cluster of the original Cluster 1. The re-cluster process successfully separates clusters with CH_4 contamination (3 and 6). The line keyed as VF shows the spectrum of the ammonia-rich regions in Virgil Fossae and surroundings (from Dalle Ore 2019). (For interpretation of the references to color in this figure, the reader is referred to the web version of this article.)

The remaining four classes show a gradient in the depth of bands at ~1.5-1.6 μm, 1.65 μm, 2 μm, and, although weak, also a variation at 1.8 μm.

FIGURE 9 HERE

Figure 9. Geographical distribution of the Cluster 1 re-cluster classes. The arrow points to the 28-km crater considered here. The color rectangles at the top correspond to the colors of the spectral traces in Figure 10. The dark diagonal line (lower left) is an artifact, and although it is nearly coincident with the linear fissure discussed in the text, it does not affect the distribution pattern of the spectral clusters. (For interpretation of the references to color in this figure, the reader is referred to the web version of this article.)

As predicted by the CH criterion index, the geographical distribution of the pixels corresponding to each cluster average is indicative of a gradient. When compared with Figure 9, it is seen that the blue Cluster 5 pixels correspond to craters, those of Cluster 4 surround Cluster 5, and pixels belonging to Clusters 1 and 2 are more widespread. Spectroscopically, Cluster 5 pixels are those with the deepest H_2O bands (Figure 6).

When comparing the cluster averages with no CH_4 in this region to the cluster average of the NH_3-rich spectra in Virgil Fossae (Dalle Ore et al. 2019), denoted here as VF (grey trace), we see that Cluster 5 (blue trace) shows the most extreme behavior, indicating an even stronger concentration of H_2O and ammoniated compounds than in the VF surroundings. Cluster 4 shows a similarly strong signature, while Cluster 1 is comparable to VF in the depth of its bands and Cluster 2 appears slightly weaker than VF.

FIGURE 10 HERE

Figure 10. Cluster averages corresponding to the re-clustering of Cluster 1. Only the clusters uncontaminated by CH_4 are shown. The orange trace is the spectrum of Nix (Cook et al. 2018), with the absorption band of the ammoniated species marked with the horizontal line. The same absorption is seen in the inverse ratio plot for Virgil Fossae (VF) and the other inverse ratio traces in this figure. The vertical spike at ~1.85 μm is an artifact. (For interpretation of the references to color in this figure, the reader is referred to the web version of this article.)

In conclusion of this section, we note that while much of the terrain in the region of the fossa-crater complex shows a small degree of spectral contamination by CH_4 frost or ice, the signature of ammoniated H_2O ice in the main trough, the flooded crater, and

surroundings is clear. As noted above, the CH_4 signature is mostly found on crater rims, as well as on the mountainous terrain to the east of the fossa.

5. Comparison with Virgil Fossae

The Virgil Fossae graben complex (~11º N, 132º E) studied in Cruikshank et al. (2019a) consists of a main trough ~300 km long that on its eastern end cuts across the north rim of Elliot crater and then disappears into the terrain on the east side of the crater. At its western end, the main trough devolves into a series of right-lateral strike-slip duplexes defining several isolated lenses that extend the structure an additional ~200 km to the southwest. Within the main trough, a distinctive red-orange pigment covers the floor for about 100 km, and then extends eastward through the trough in a narrow band along the south wall. The south wall is 2.8 km above the floor, and the north wall has a height of ~1.8 km (Schenk et al. 2018). The color and the main structural and topographic features, including an altitude profile along the floor of the main trough, are given in Cruikshank et al. (2019).

The distribution of the colored, ammoniated H_2O within the Virgil Fossae troughs and in the surrounding terrain, particularly to the south, suggests that the principal source of the material that appears to lay along the floor of the main trough produced a fountain of cryoclastic material that has covered several thousand square kilometers with a mantling layer of unknown thickness. Simple ballistic considerations of such explosive ejection of cryoclastics show that with an ejection velocity of just a few hundred m s^{-1}, material could travel some 200 km. Elsewhere in the main trough, in the direction of Elliot crater, the same cryolava appears to have debouched along the fault defining the south wall, flowed a short distance perpendicular to the wall, and frozen in place. Although there is no definitive evidence for fountaining emplacement of cryoclastic materials in the region of study in the present paper, the morphology of the deposit of ammoniated H_2O around the fissure is similar to that of pyroclastic deposits on the Moon in the crater Alphonsus, the Schrodinger basin, and elsewhere (e.g., Gaddis et al. 2000).

6. Ammoniated materials and age of emplacement

Spectral images from the New Horizons LEISA instrument show that much of the subject region in Viking Terra, in addition to carrying the red-orange pigment, is covered with H_2O ice that also has the spectral signature of NH_3 or an ammoniated compound. Such a signature appears as a depression on the long wavelength side of the 2.0-μm band that varies in width and position from one cluster average to another. This behavior is suggestive of the possible presence of more than one ammoniated species. Owing to the signal precision of the data and the limited availability of laboratory data, the nature of the ammonia is unclear; it could be pure NH_3 ice, an ammonia hydrate (NH_3•$2H_2O$, NH_3•H_2O, or $2NH_3$•H_2O), or an ammoniated salt (e.g., NH_4Cl) (Dalle Ore et al., 2019). As Cruikshank et al. (2019a) have shown, pure NH_3 is unlikely because if it is frozen as a mixture with liquid H_2O, one or more of the hydrate forms would result.

The ammonia molecule, ammonia hydrates and ammoniated salts are susceptible to destruction by ultraviolet light and charged particles, both of which occur at Pluto's surface. Lyman-α radiation (121.6 nm, 10.19 eV) from direct sunlight and from backscattering from the interplanetary medium destroys NH_3, for which the ionization energy is 10.2 eV. Lyman- α is modulated by CH_4 in Pluto's atmosphere; the CH_4 content is variable over the planet's year and on million-year time-scales (Bertrand et al. 2019), so the flux reaching the surface ranges from ~0.01% to 10% of the incoming flux. Direct solar ultraviolet at longer wavelengths is not strongly absorbed by atmospheric CH_4 and readily ionizes NH_3. The penetration depth of UV photons is a few micrometers (Bennett et al. 2013). Galactic cosmic rays (GCR) penetrate Pluto's icy surface to depths of a few meters, undergoing hadronic interactions and producing secondary particles that in turn have further interactions, depending on their energy, ionizing the paths they traverse. A model of GCR penetration of Pluto's surface is presented in Cruikshank et al. (2019a), with the result that in the uppermost meter the energy deposited is ~10^7 eV g^{-1} s^{-1}. This energy is sufficient to break at least one N-H bond in every NH_3 molecule in that layer in ~1.1 x 10^9 y. The charged particle flux from the Sun incident on Pluto's surface is variable and not well characterized. Both primary and secondary particles can readily destroy NH_3, but only to depths of a few micrometers.

Laboratory work by Loeffler et al. (2010a,b) demonstrated that the 2.2-μm band considered here is readily destroyed by 100 keV protons in an NH_3:H_2O ice mixture at temperatures >120 K, but at lower temperatures characteristic of Pluto and its satellites, the destruction is slower. They estimated that on Charon, if the ammonia signature in its spectrum is representative of ammonia hydrates, about 40% or more of the original ammonia has been removed from the optical surface by impinging protons within the age of the Solar System.

For pure NH_3 the destruction mechanism and rates are reasonably well-known, although as noted, the pure form is unlikely to exist at the surface because of its tendency to form hydrates in the presence of H_2O. More measurements of photon and charged particle destruction of ammonia hydrates are needed, and there is a special need for radiation studies of ammoniated salts.

After an evaluation of the available environmental energy sources, Cruikshank et al. (2019a) concluded that the age of the NH_3 spectral signature in the Virgil Fossae exposure is in the broad range 10^4 to 10^9 y, but in any case possibly less than the age of the planet. The value 10^4 y corresponds to pure NH_3 in H_2O, which, as described above, is unlikely to occur from a chemical point of view. This range probably also applies to the flooded terrain considered here, and may be relevant to all exposures of ammonia-bearing water ice on Pluto, including those yet to be elaborated.

We conclude this section by noting that the 2.2-μm band of an ammoniated material is prominent on Pluto's small satellites Nix and Hydra (Cook et al. 2018), which are entirely unprotected from the destructive effects of the space environment. These bodies are too small and cold to have internal processes to refresh their surfaces endogenically. The

persistence of the spectral signature on Nix and Hydra, as well as Charon, presumably for the age of the Solar System, thus is a conundrum currently lacking a clear explanation.

7. Discussion

It is clear in the map of H_2O ice distribution in Figure 2 that water ice is widespread in a patchy distribution throughout Viking Terra, in many cases associated with distinctive topographic structures. In addition to the region of study in the present paper, H_2O ice is seen in the Inanna and Dumuzi Fossae, much of Bird Planitia, and along both sides of the north-south trending mountain range at the east margin of Viking Terra. When compared with the enhanced color map of the same area in Figure 1, it is seen that the H_2O distribution and the red-brown color are coincident in all of these exposures. This coincidence is compelling evidence that the ice is the carrier of the pigment, as was concluded in the study of Virgil Fossae (Cruikshank et al. 2019a,b).

The H_2O ice distributed throughout this region may have more than a single origin. In expanses where there is no clear association with topographic structures it is possible that the ice represents Pluto's crustal material that has no overcoat of the usual, mobile, volatile ices (N_2, CH_4, CO). Deposition and sublimation of those ices are variable over Pluto's annual and Milancović timescales, and in addition it is conceivable that wind scouring at times of greater atmospheric density could also lay bare some regions of the crust. The present epoch may represent a time when some of the original crust is exposed. In this scenario it is implied that the pigment is an integral component of the H_2O ice crust, or that the coloration occurred at a later time, perhaps by exposure to sunlight and charged particles in Pluto's space environment. Whether the same putative original ice crust carries an ammoniated component is not yet clear, pending further investigation of the spectral signatures of the relevant regions.

In other regions associated with structures indicating the formation of impact craters and graben, such as those features described in this paper, the colored H_2O appears to have been deposited on the surface by effusion from one or more sources within the crust. In the fossa trough and adjacent flooded crater described here, as in Virgil Fossae and surroundings, the colored H_2O ice appears to have been deposited from a nearby source or sources. The preponderance of evidence is in favor of effusive cryovolcanism and minor cryoclastic eruptions in a few events that carried the colored fluid from a subsurface source. As in Virgil Fossae, debouchement of cryolava is likely to have occurred along the normal faults defining the trough described here, and perhaps along fractures in the floor of the flooded 28-km impact crater. Lesser amounts of crater filling and smaller amounts of the same cryolava appear in the same region, and may also represent the emergence of the cryolava.

In the scenario of effusive cryovolcanism, as with the possible exposure of primitive crust, the pigment is presumed to be a native component of the cryolava. The issue of the ammoniated material in the cryolava, and its limited (but largely unquantified) durability in the surface space environment is used in support of the relative youth of the effused material in the trough and crater discussed here, and the possible presence of similar

ammoniated material in original crust is not yet clear. For the purposes of the present paper, and pending further study of the lifetime of plausible ammoniated materials in Pluto's cryolava we adopt the basic argument formulated in the Virgil Fossae study and tentatively conclude that the deposit considered here was emplaced of order ≤ 1 Gy ago.

In this paper we have drawn comparisons between the Viking Terra features and Virgil Fossae from the earlier study by Cruikshank et al. (2019a). Attention was initially drawn to Virgil Fossae by the nearly unique color both in the main trough and in the immediate surroundings, a color having only a few smaller exposures (e.g., Beatrice Fossae) on the hemisphere of Pluto imaged with high resolution by New Horizons (Olkin et al. 2017). The varied and widespread coloration of Pluto's ices is attributed to refractory complex organic compounds (tholins) formed by photochemical reactions in the atmosphere and precipitated to the surface (Cheng et al. 2017; Grundy et al. 2018), and more directly by photolysis and radiolysis of CH_4 and N_2 in the surface ices (e.g., Cruikshank et al. 2016). In view of the special colors in Virgil Fossae, Cruikshank et al. (2019b) proposed that complex organics present in a subsurface fluid reservoir that supplied the cryolava in the fossa trough and surroundings by cryoclastic eruptions constitute a third source of tholins now seen on the planet's surface. The unique color of the Virgil Fossae tholin may represent a composition different from that of other widespread surface exposures, or it might be an indication of its relative chemical immaturity, perhaps consistent with the relatively recent deposition on the surface inferred from its distribution in and around the fossae complex. Continued changes through chemical interaction with Pluto's space environment may alter the color over the long term, perhaps making it less distinctive in comparison with the red-brown color of much of the planet's surface.

8. Summary and Conclusions

A prominent fossa and adjacent 28-km diameter crater in Viking Terra show evidence of filling by a fluid composed primarily of water carrying a red-brown pigment and an ammonia-bearing compound. The morphology and color are evident in the direct high-resolution images from New Horizons, and the spectral signatures of H_2O and NH_3 are extracted from spectral maps of the region made with the LEISA instrument. Material of similar color and composition is seen in an irregular distribution in the area surrounding the trough and crater. The spectral signature of NH_3 is attributed to ammoniated compounds in the ice, probably an ammonia hydrate ($NH_3 \bullet nH_2O$) or an ammoniated salt such as NH_4Cl, which may be responsible for a similar spectral band in the spectrum of Pluto's small satellite Nix (Cook et al. 2018).

The favored explanation for the filling material in the fossa and crater is a cryovolcanic event or events in which a cryolava consisting of liquid H_2O carrying a pigment and ammoniated compounds emerged along the normal faults defining the trough, and possibly through the fractured crust in the crater. Adjacent exposure of the same material probably emerged through other faults. The widespread occurrence of H_2O-rich colored deposits throughout Viking Terra may have come from a single or multiple subsurface sources in one or more effusive eruptions in this tectonically deformed region of Pluto's surface.

Acknowledgment

This work was supported by NASA's New Horizons project. We thank NASA and the entire New Horizons team for their hard work leading to a spectacularly successful Pluto system encounter. B. Schmitt acknowledges France's Centre National d'Etudes Spatiales (CNES) for its financial support through its "Système Solaire" program.

References

Bennett, C.J., Pirim, C., Orlando, T.M., 2013. Space-weathering of solar system bodies: a laboratory perspective. Chem. Rev. 113, 9086–9150.

Bertrand, T., Forget, F., Umurhan, O. M., Moore, J. M., Young, L. A., Protopapa, S., Grundy, W. M., Schmitt, B., Dhingra, R. D., Binzel, R. P., Earle, A. M., Cruikshank, D. P., Stern, S. A., Weaver, H. A., Ennico, K., Olkin, C. B., and the New Horizons Science Team, 2019. The CH_4 cycles on Pluto over seasonal and astronomical timescales. 2019 Icarus 329, 148-165.

Bryan, S. E., Peate, I. U., Peate, D. W. et al., 2010. The largest volcanic eruptions on Earth. Earth Science Reviews 102, 207-229.

Calinski. Y., Harabasz, J., 1974. A dendrite method for cluster analysis. Commun. Stat. 3, 1-27.

Cheng, A.F., Summers, M. E., Gladstone, G. R. et al., 2017. Haze in Pluto's atmosphere. Icarus 290, 112–133.

Cook, J. C., Dalle Ore, C. M., Protopapa, S., Binzel, R. P., Cartwright, R., Cruikshank, D. P., Earle, A., Grundy, W. M., Ennico, K., Howett, C., Jennings, D. E., Lunsford, A. W., Olkin, C. B., Parker, A. H., Philippe, S., Reuter, D., Schmitt, B., Stansberry, J. A., Stern, S. A., Verbiscer, A., Weaver, H. A., Young, L. A., 2018. Composition of Pluto's small satellites: Analysis of New Horizons spectral images. Icarus 315, 30-45.

Cook, J. C., Dalle Ore, C. M., Protopapa, S. et al., 2019. The distribution of H_2O, CH_3OH, and hydrocarbon ices on Pluto: Analysis of New Horizons spectral images. Icarus 331, 148-169.

Cruikshank, D. P., Clemett, S. J., Grundy, W. M. et al., 2016. Pluto and Charon: The non-ice surface component. Lunar Planet. Sci. Conf. 47th. Abstract #1700.

Cruikshank, D. P., Umurhan, O. M., Beyer, R. A., Schmitt, B., Keane, J. T., Runyon, K. D., Atri, D., White, O. L., Matsuyama, I., Moore, J. M., Sandford, S. A., Singer, K., Grundy, W. M., Dalle Ore, C. M., Cook, J. C., Bertrand, T., Stern, S. A., Olkin, C. B., Weaver, H. A., Young, L. A., Spencer, J., Lisse, C. M., Binzel, R. P., Earle, A., Robbins, S., Gladstone, G. R., Ennico, K., Cartwright, R., 2019a. Recent cryovolcanism in Virgil Fossae on Pluto. Icarus 330, 155-168.

Cruikshank, D. P., Materese, C. K., Pendleton, Y. J., Boston, P. J., Grundy, W. M., Schmitt, B., Lisse, C. M., Runyon, K. D., Keane, J. T., Beyer, R. A., Summers, M. E., Scipioni, F., Stern, S. A., Dalle Ore, C. M., Olkin, C. B., Young, L. A., Ennico, K., Weaver, H. A., Bray, V. J., 2019b. Prebiotic chemistry of Pluto. Astrobiology 17, No. 7 (July).

Dalle Ore, C., M., Cruikshank, D. P., Protopapa, S., Scipioni, F., McKinnon, W. B., Cook, J. C., Grundy, W. M., Stern, S. A., Weaver, H. A., Verbiscer, A., Olkin, C. B., Young, L. A., Ennico, K., Schmitt, B. and the New Horizons Science Team, 2019. Detection of ammonia on Pluto's surface in a region of geologically recent tectonism. Sci. Adv. 5:eaav5731, 29 May.

Gaddis, L. R., Hawke, B. R., Robinson, M. S., Coombs, C., 2000. Compositional analysis of small lunar pyroclastic deposits using Clementine multispectral data. J. Geophys. Res.: Planets, 105 (E2), 4245-4262.

Grundy, W., Bertrand, T., Binzel, R. P., Buie, M. W., Buratti, B. J., Cheng, A. F., Cook, J.C., Cruikshank, D. P., Devins, S. L., Dalle Ore, C. M., Earle, A. M., Ennico, K., Forget, F., Gao, P., Gladstone, G. R., Howett, C. J. A., Jennings, D. E., Kammer, J. A., Lauer, T. R., Linscott, I. R., Lisse, C. M., Lunsford, A. W., McKinnon, W. B., Olkin, C. B., Parker, A. H., Protopapa, S., Quirico, E., Reuter, D. C., Schmitt, B., Singer, K., N., Spencer, J., A., Stern, S. A., Strobel, D. F., Summers, M. E.,Weaver, H., A., Weigle, G. E. II, Wong, M. L., Young, E. F., Young, L. A., Zhang, X., 2018. Pluto's haze as a geological material. Icarus 314, 232-245.

Keane, J. T., Matsuyama, I., Kamata, S., Steckloff, J. K., 2016. Reorientation and faulting of Pluto due to volatile loading within Sputnik Planitia. Nature 540, 90–93.

Loeffler, M. J., Raut, U., Baragiola, R. A. 2010a. Radiation chemistry in ammonia-water ices. J. Chem. Phys. 132, 054508

Loeffler, M. J., Baragiola, R. A. 2010b. Photolysis of solid NH_3 and NH_3–H_2O mixtures at 193 nm. J. Chem. Phys. 133, 214506.

Martin, B. S., Pletcovic, H. L., Reidel, S. P. 2005. Goldschmidt Conference 2005: Field trip guide to the Columbia River Basalt Group. Pacific Northwest National Laboratory, PNNL-15221. doi:10.2172/15016367.

Martin, C. R., Binzel, R. P. 2020 Ammonia-water freezing as a mechanism for recent cryovolcanism on Pluto. Icarus (in press).

Olkin, C. B., Spencer, J. R., Grundy, W. M., Parker, A. H., Beyer, R. A., Schenk, P. M., Howett, C., J. A., Stern, S. A., Reuter, D. C., Weaver, H. A., Young, L. A., Ennico, K., Binzel, R. P., Buie, M. W., Cook, J. C., Cruikshank, D. P., Dalle Ore, C. M., Earle, A. M., Jennings, D. E., Singer, K. N., Linscott, I. E., Lunsford, A. W., Protopapa, S.,

Schmitt, B., Weigle, E., 2017. The color of Pluto from New Horizons. Astron. J. 154:258 (13pp) December.

Protopapa, S., Grundy, W.M., Reuter, D.C., et al., 2017. Pluto's global surface composition through pixel-by-pixel Hapke modeling of New Horizons Ralph/LEISA data. Icarus, 287, 218-228.

Schenk, P. M., Beyer, R. A., McKinnon, W. B., et al., 2018. Basins, fractures and volcanoes: Global cartography and topography of Pluto from New Horizons. Icarus 314, 400-433.

Schmitt, B., Philippe, S., Grundy, W. M., et al., 2017. Physical state and distribution of materials at the surface of Pluto from New Horizons LEISA imaging spectrometer. Icarus, 287, 229-260.

Singer, K. N., White, O. L., Schenk, P. M. et al., 2016. Pluto's putative cryovolcanic constructs. 47th LPSC abstract 2276.pdf.

Singer, K. N., Schenk, P. M., White, O. L. et al., 2018. Cryovolcanism on Pluto from the New Horizons flyby. LPI Contribution No. 2045, id.2012, from Cryovolcanism in the Solar System Workshop, June, 2018, Houston, TX.

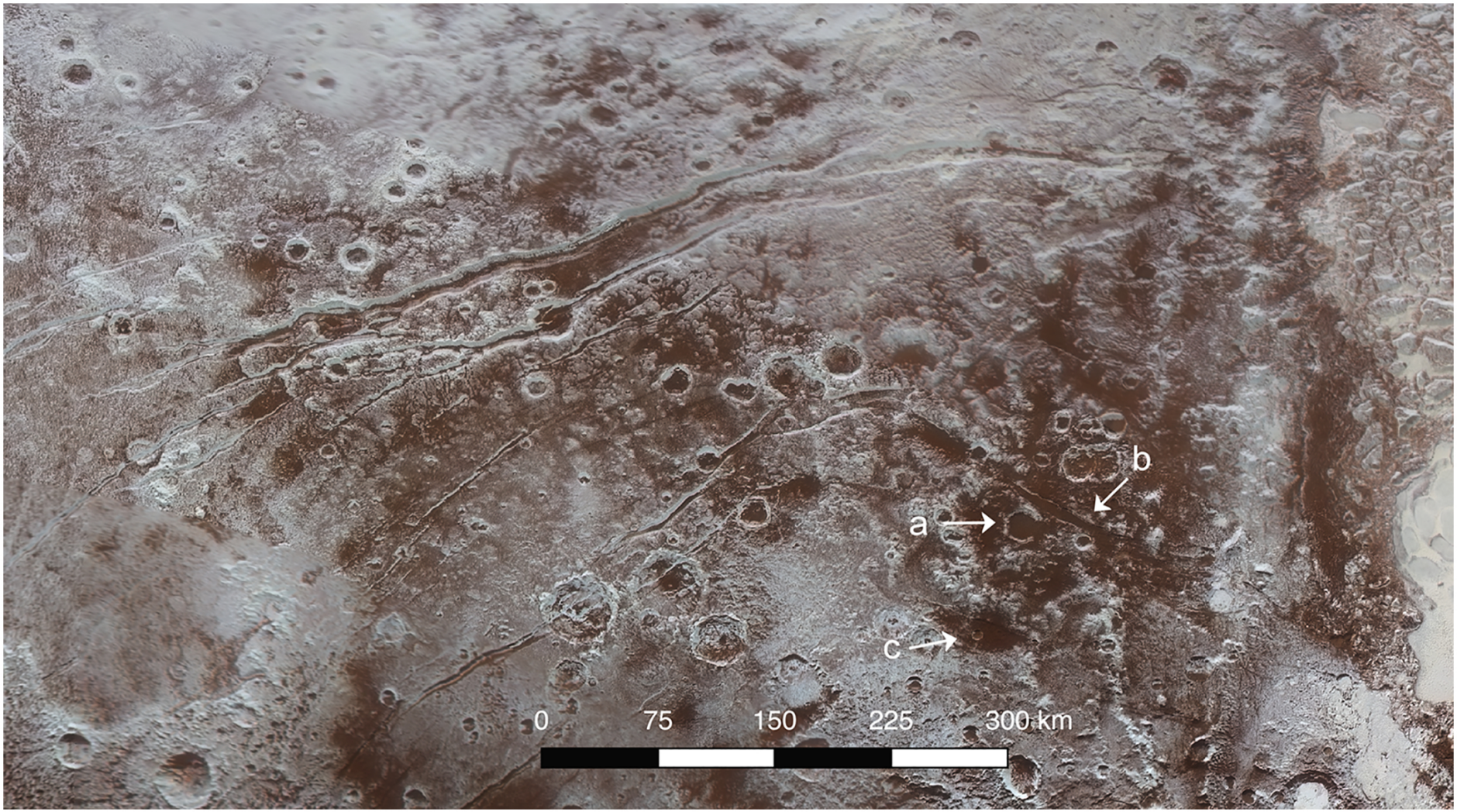

Figure 1

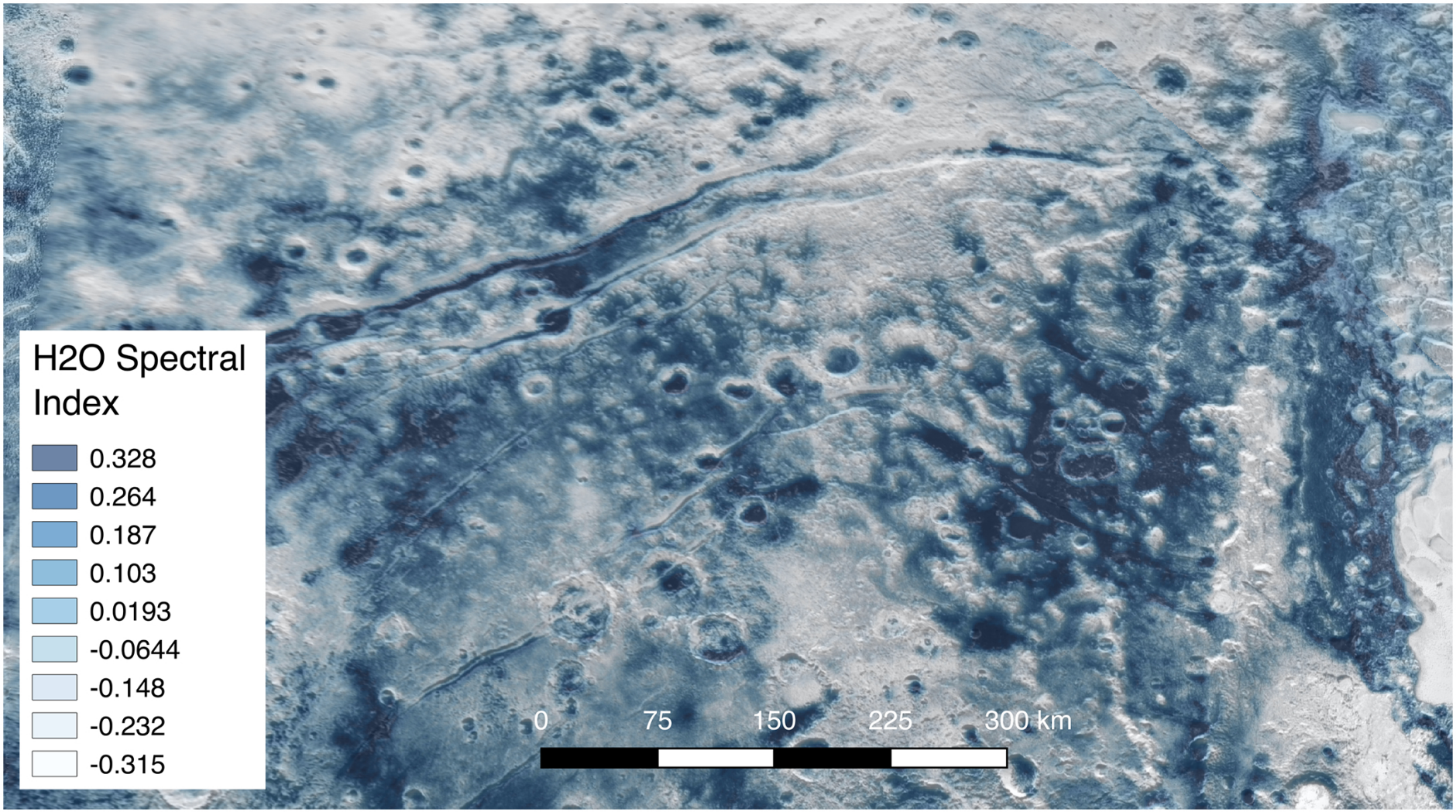
H2O Spectral Index
0.328
0.264
0.187
0.103
0.0193
-0.0644
-0.148
-0.232
-0.315
0
75
150
225
300 km

Figure 2

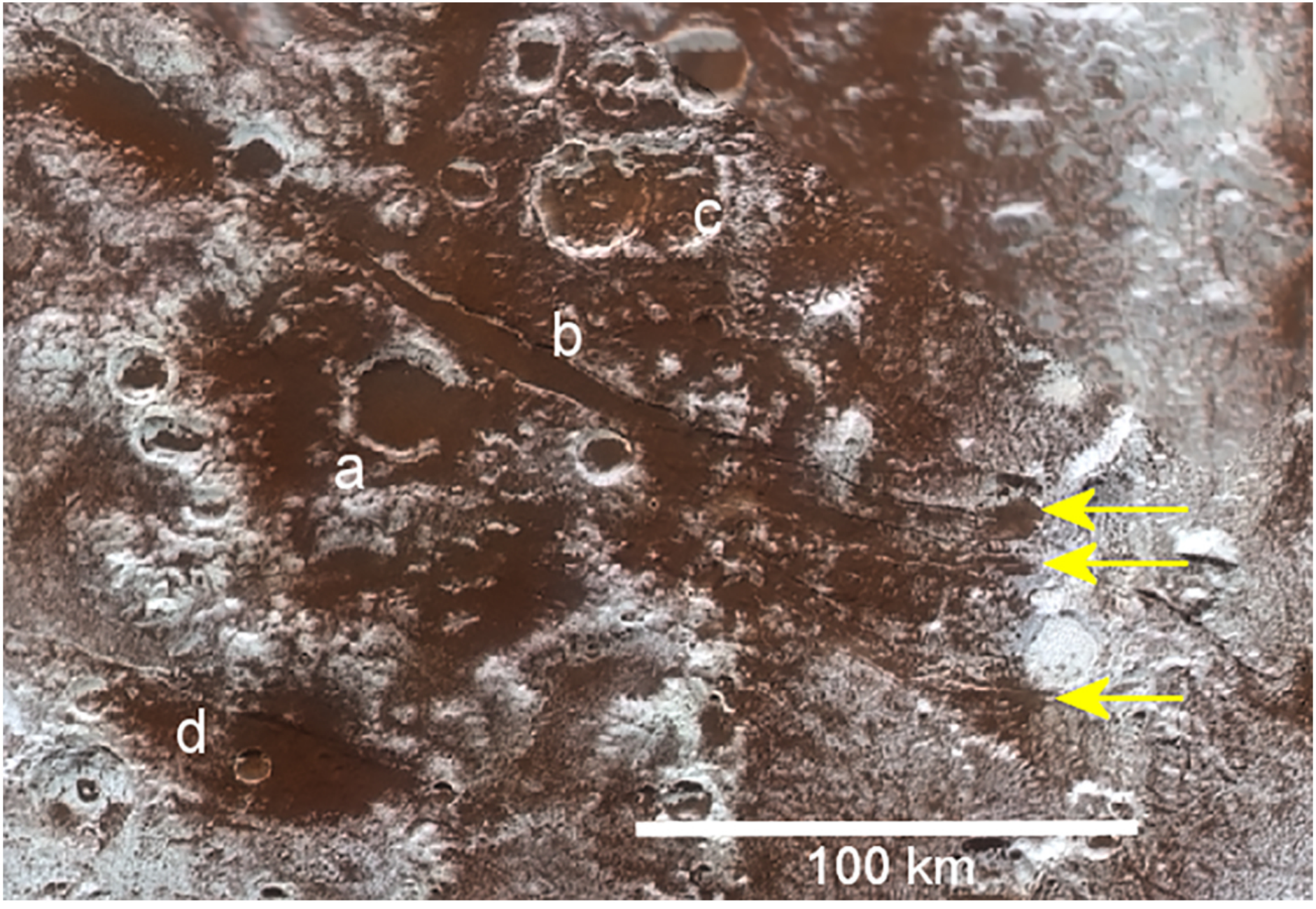

Figure 3

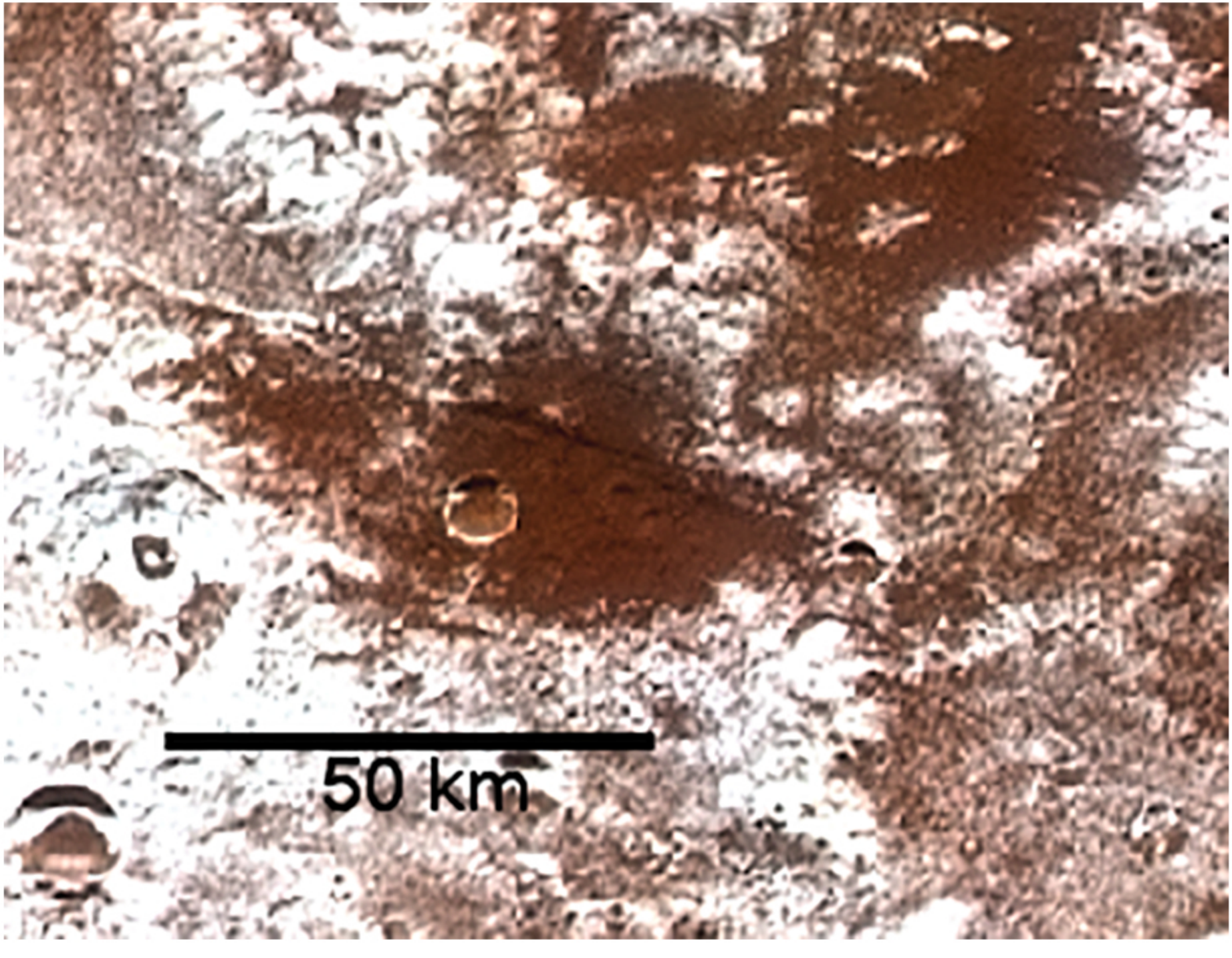

Figure 4

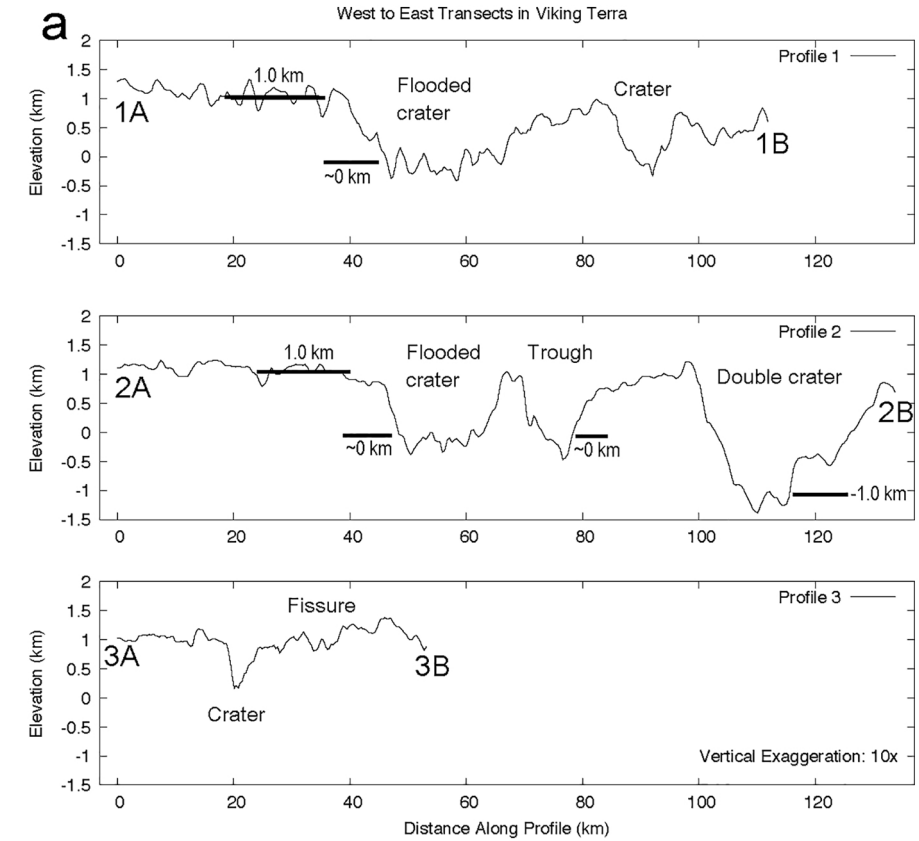
a
West to East Transects in Viking Terra
Profile 1
1.0 km
Flooded crater
Crater
1A
1B
~0 km
Profile 2
1.0 km
Flooded crater
Trough
Double crater
2A
2B
~0 km
~0 km
-1.0 km
Profile 3
Fissure
3A
3B
Crater
Vertical Exaggeration: 10x
Elevation (km)
Distance Along Profile (km)

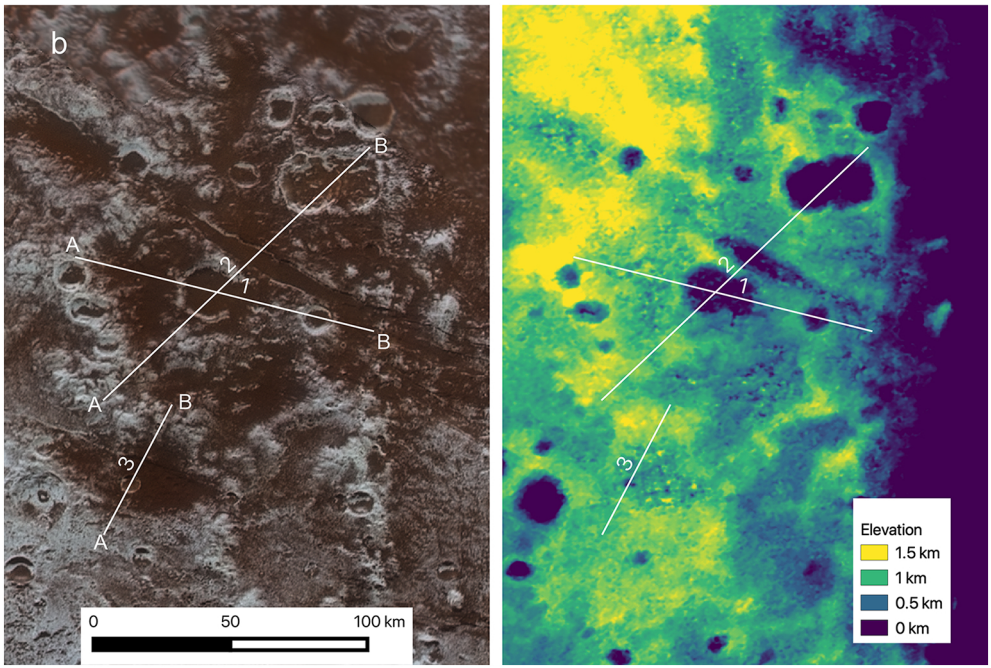
b
A
B
1
2
3
0
50
100 km
Elevation
1.5 km
1 km
0.5 km
0 km

Figure 5

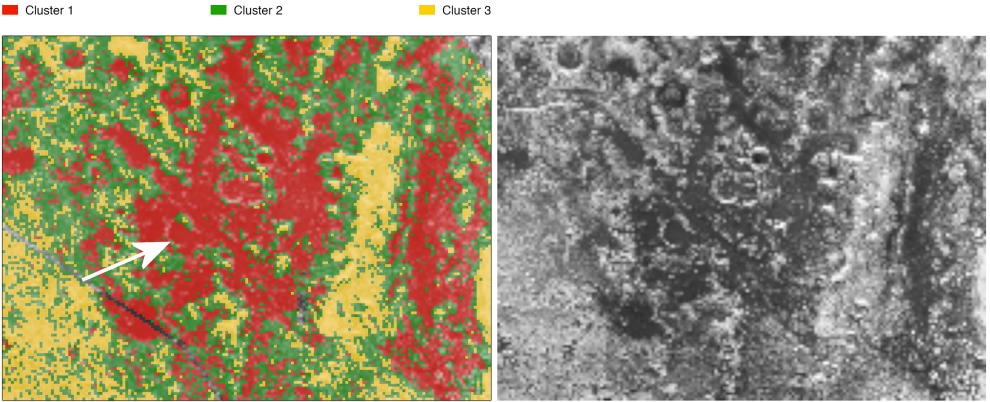

Figure 6

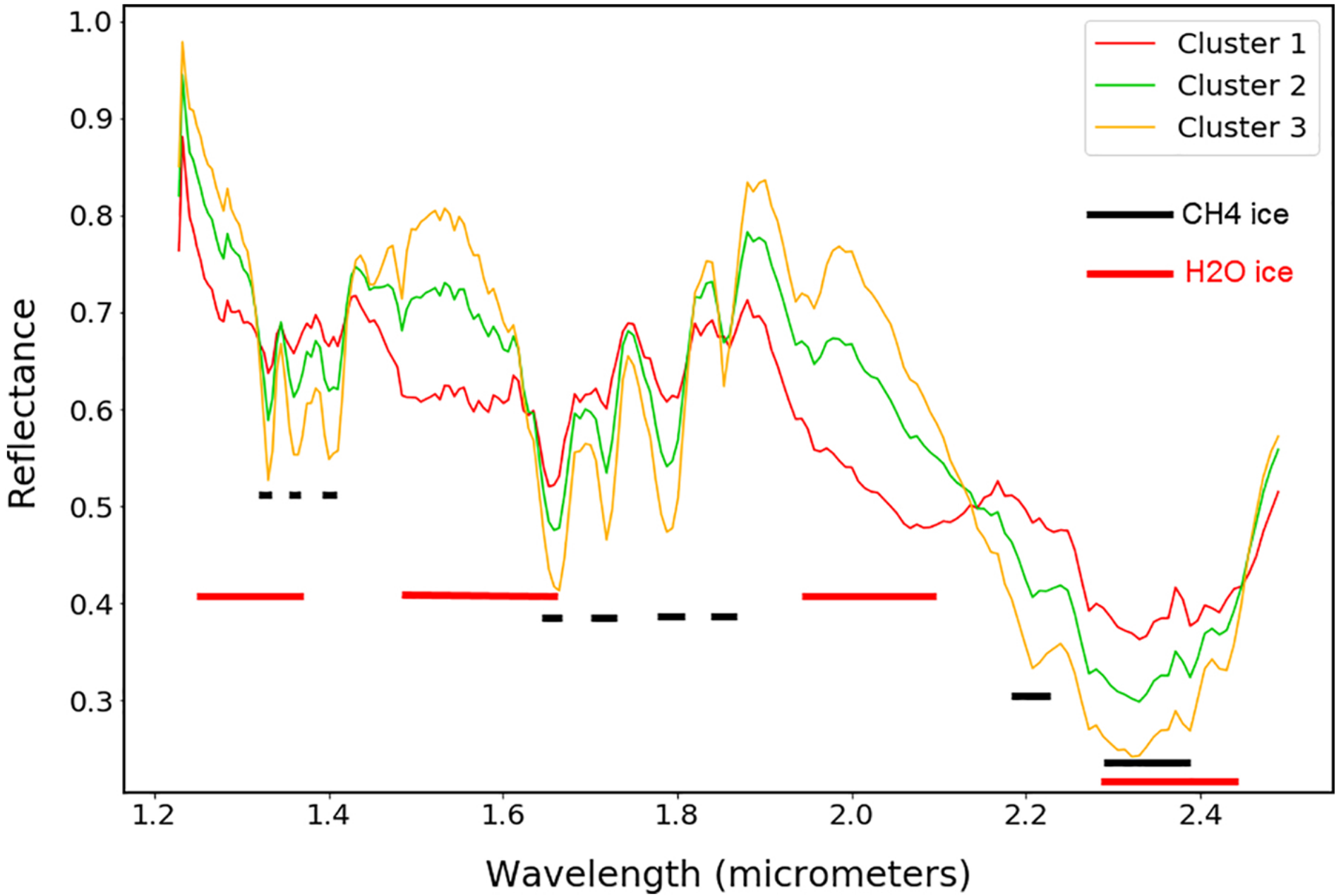
Cluster 1
Cluster 2
Cluster 3
CH4 ice
H2O ice
Reflectance
Wavelength (micrometers)
1.0
0.9
0.8
0.7
0.6
0.5
0.4
0.3
1.2
1.4
1.6
1.8
2.0
2.2
2.4

Figure 7

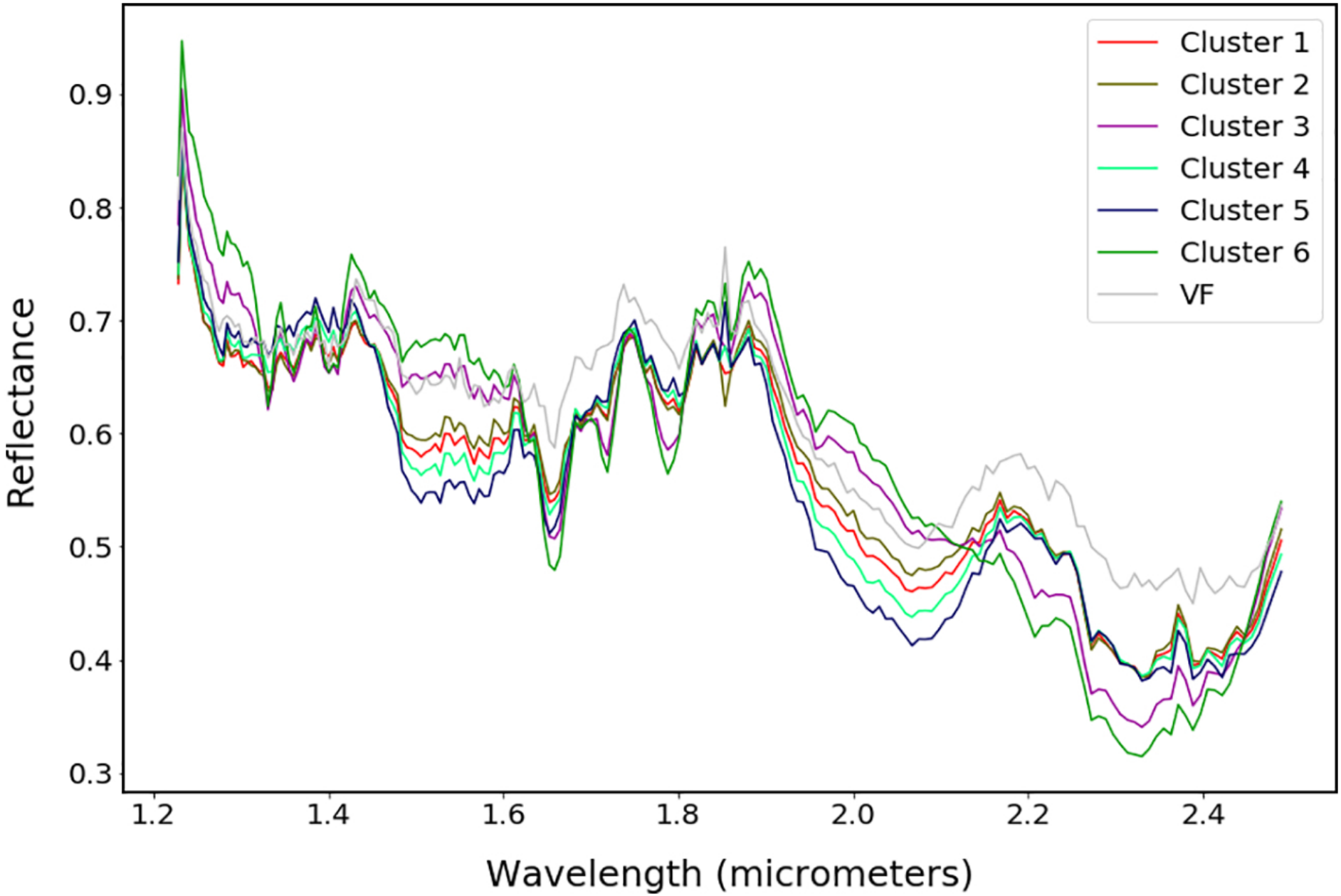
Cluster 1
Cluster 2
Cluster 3
Cluster 4
Cluster 5
Cluster 6
VF
Reflectance
0.9
0.8
0.7
0.6
0.5
0.4
0.3
1.2
1.4
1.6
1.8
2.0
2.2
2.4
Wavelength (micrometers)

Figure 8

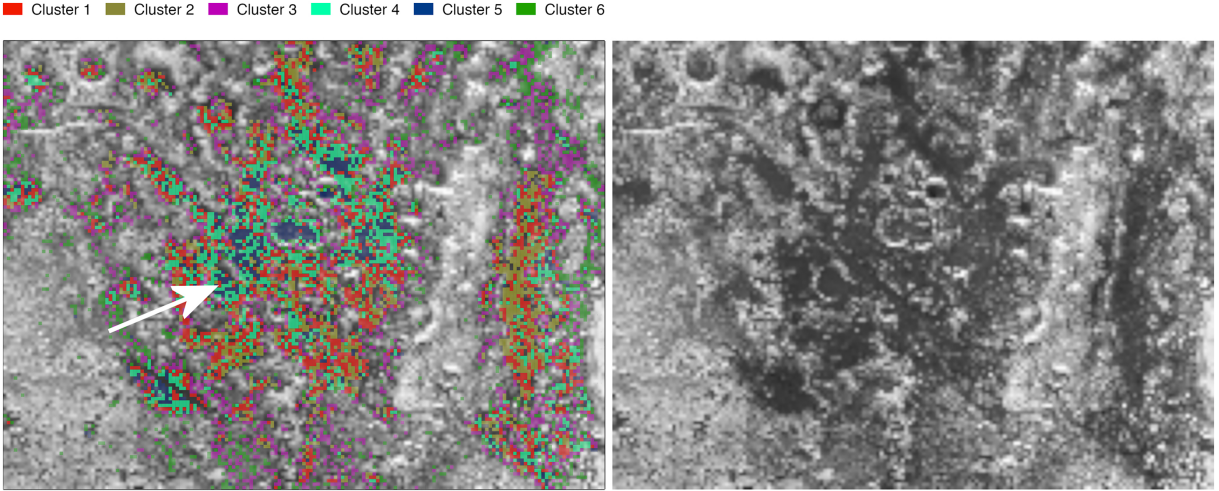

Figure 9

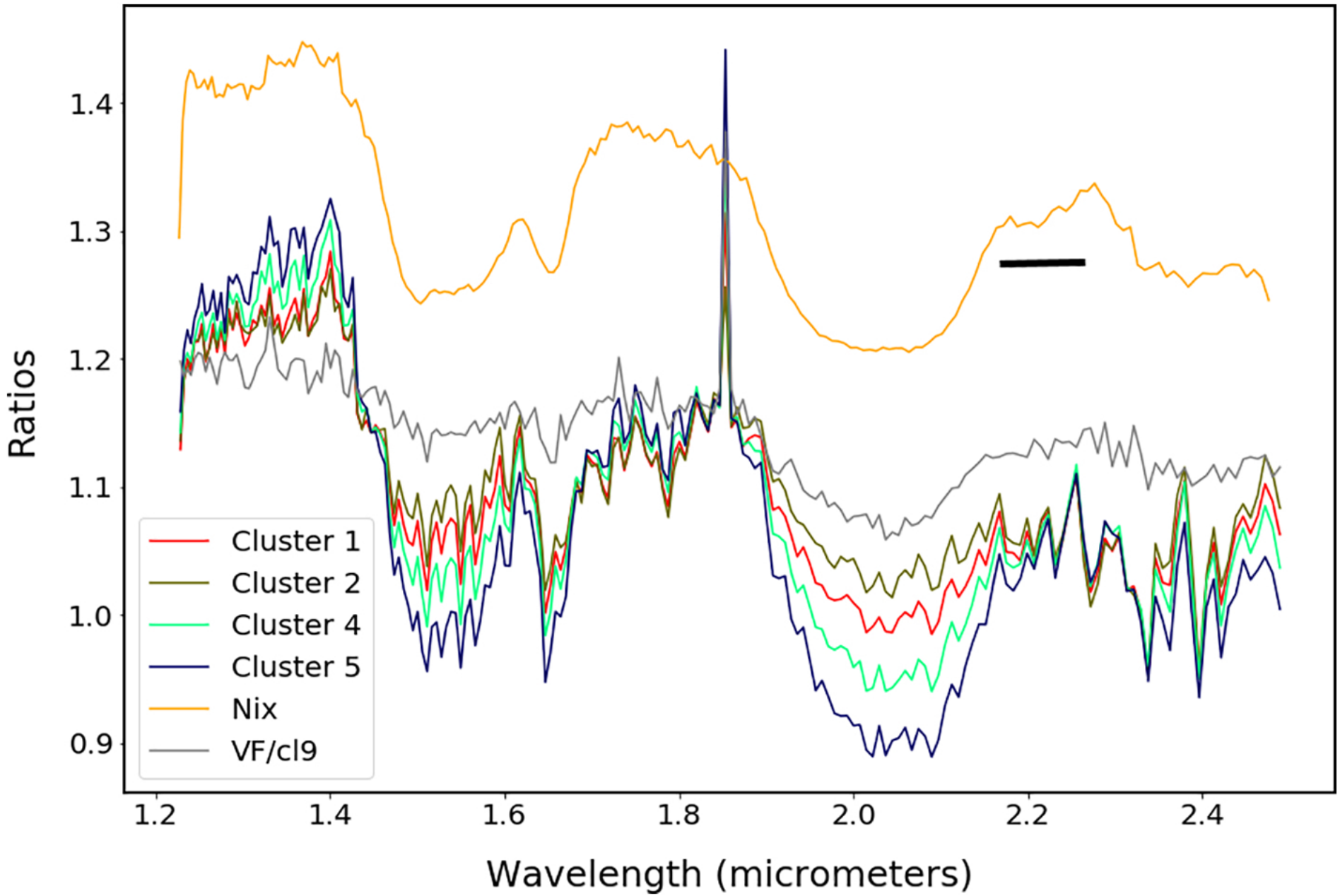
Ratios
1.4
1.3
1.2
1.1
1.0
0.9
1.2
1.4
1.6
1.8
2.0
2.2
2.4
Wavelength (micrometers)
Cluster 1
Cluster 2
Cluster 4
Cluster 5
Nix
VF/cl9

Figure 10